

LES of a Converging–Diverging Channel Performed with the Immersed Boundary Method and a High-Order Compact Discretization

Mariusz Ksiezyk and Artur Tyliczszak

Abstract The paper presents the results of numerical simulations of an incompressible flow in a converging–diverging channel performed with Large Eddy Simulation (LES) combined with the immersed boundary (IB) method. The computations are carried out using a high-order code with the spatial discretization based on the compact difference method for half-staggered meshes. IB method is implemented in the so-called direct forcing approach with a second-order interpolation near the boundaries. Two relatively new subgrid models are used in the simulations, i.e. the model proposed by Vreman, *Phys Fluids* 16:3670–3681, 2004, [1] and the model proposed by Nicoud et al., *Phys Fluids* 23:193–202, 2011, [2]. It is demonstrated that both of them perform well and there is no evident advantage for either of them. The mean and r.m.s velocity profiles agree with exemplary DNS data.

1 Introduction

Undoubtedly, from the point of view of a solution accuracy none of the discretization methods may compete with the spectral and pseudo-spectral methods which are regarded as the most accurate [3]. The weak point of these approaches is that they can only be applied in rather simple computational domains and with nodes distribution and boundary conditions enforced by the type of the method. The high-order compact difference methods [4] seem to give more possibilities regarding non-uniformity of the computational meshes, selection of the boundary conditions or shapes of computational domains. They are successfully applied on non-uniform meshes and in irregular domains [5–7]. However, such applications require domain division, normalisation, coordinate transformations, etc., which are not trivial tasks. Possibly the easiest solution allowing to use the compact methods in complicated domains is to combine them with the so-called Immersed Boundary (IB) method. Application of

M. Ksiezyk (✉) · A. Tyliczszak
Czestochowa University of Technology, Czestochowa, Poland
e-mail: ksiezykm@imc.pcz.czyst.pl

A. Tyliczszak
e-mail: atyl@imc.pcz.czyst.pl

this approach seems to be relatively easy and very efficient [8]. The Navier–Stokes equations are solved on Cartesian regular grids with arbitrary boundaries or arbitrary objects embedded directly on the grid points. The influence of such objects on the flow field is enforced by body force terms added to the Navier–Stokes equations [8, 9]. The present work focuses on application of the high-order compact method with IB approach for LES of incompressible flows. The computations are performed using two well-known and relatively new subgrid models proposed by Vreman [1] and Nicoud et al. [2] and the obtained solutions agree very well with DNS data.

2 Mathematical Model and Numerical Algorithm

Flow of an incompressible fluid is governed by the continuity equation and Navier–Stokes equations which in the framework of LES combined with the IB method are given as:

$$\frac{\partial \bar{u}_i}{\partial x_i} = 0 \quad (1)$$

$$\frac{\partial \bar{u}_i}{\partial t} + \bar{u}_j \frac{\partial \bar{u}_i}{\partial x_j} = -\frac{1}{\rho} \frac{\partial \bar{p}}{\partial x_i} + \frac{\partial}{\partial x_j} \left((v + \nu_t) \left(\frac{\partial \bar{u}_i}{\partial x_j} + \frac{\partial \bar{u}_j}{\partial x_i} \right) \right) + f_{IB} \quad (2)$$

where the bar symbol denotes spatial filtering [10], u_i are velocity components, ρ is constant density, p —pressure, ν , ν_t —kinematic and eddy viscosity and f_{IB} denotes source terms which will be used to force zero values of velocity at the domain boundaries or inside the bodies embedded on the computational nodes.

2.1 Subgrid Modelling

In this paper we compare the results obtained using the models proposed by Vreman [1] and Nicoud et al. [2]. These models belong to the family of the so-called eddy viscosity models and hence their implementation relies on calculation of the ν_t which is then added to the kinematic viscosity as in Eq. (2). In the case of the model proposed by Vreman [1] ν_t is computed as:

$$\nu_t = C \sqrt{\frac{B_\beta}{\alpha_{ij} \alpha_{ij}}} \quad (3)$$

$$B_\beta = \beta_{11} \beta_{22} - \beta_{12}^2 + \beta_{11} \beta_{33} - \beta_{13}^2 + \beta_{22} \beta_{33} - \beta_{23}^2 \quad (4)$$

$$\alpha_{ij} = \frac{\partial \bar{u}_j}{\partial x_i}, \quad \beta_{kl} = \Delta^2 \alpha_{mk} \alpha_{ml} \quad (5)$$

where the constant in (3) is taken as $C = 2.5 \times 10^{-2}$ [1]. The LES filter width is computed as $\Delta = (\Delta x \Delta y \Delta z)^{1/3}$ where Δx , Δy , Δz are the mesh spacings.

The model proposed by Nicoud et al. [2] is commonly known as σ -model. In the case we compute ν_t as follows:

$$\nu_t = (C_\sigma \Delta)^2 D_\sigma \tag{6}$$

$$D_\sigma = \frac{\sigma_3(\sigma_1 - \sigma_2)(\sigma_2 - \sigma_3)}{\sigma_1^2} \tag{7}$$

where the model constant is $C_\sigma = 1.35$ [2] and $\sigma_1 \geq \sigma_2 \geq \sigma_3 \geq 0$ are the singular values of the matrix

$$G = g^t g \quad \text{with} \quad g_{ij} = \frac{\partial \bar{u}_i}{\partial x_j} \tag{8}$$

Above models share features desirable in modelling of turbulent flows, i.e. they yield zero eddy viscosity close to a solid wall, in laminar flows or in pure shear regions.

2.2 Description of the Flow Solver

The set of Eqs.(1)–(2) is solved using the numerical code (SAILOR) which is an academic high-order flow solver based on the low Mach number approximation. The solution algorithm in the SAILOR code is based on the projection method in which the pressure is computed from the Poisson equation. The time advancement of Eq. (2) is performed with a predictor–corrector method with the help of the second-order Adams–Bashforth and Adams–Moulton methods. The spatial discretization is based on sixth-order compact differencing developed for half-staggered meshes (see Fig. 1) in the Cartesian coordinate system. In the present paper, the SAILOR code is used together with the IB method which is briefly presented in the next subsection.

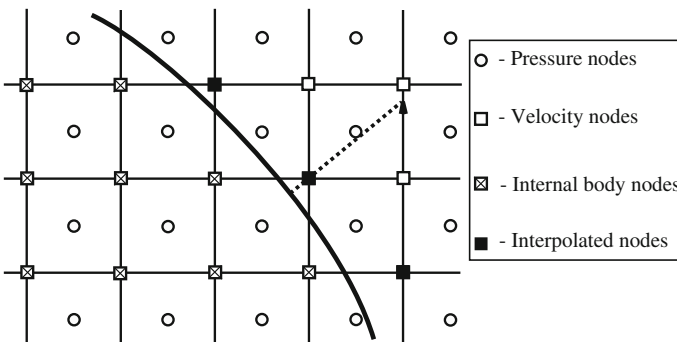


Fig. 1 Linear velocity interpolation method

2.3 Immersed Boundary (IB) Method

In general, there are two options of the IB method called feedback forcing method [11] and direct forcing method [8]. They differ in the evaluation of the forcing term. In this work the latter approach is implemented which seems to be simpler and more efficient. Interested reader is referred to [12] where all details and variants of IB methods may be found. Here, we limit the description to the definition of the forcing term used in the predictor step together with the second-order Adams–Bashforth method. In this case the term f_{IB} is defined as:

$$f_{IB} = \frac{u_{WALL} - \bar{u}_i^n}{\Delta t} - \left[\frac{3}{2} Res(\bar{u}^n) - \frac{1}{2} Res(\bar{u}^{n-1}) \right] + \frac{1}{\rho} \frac{\partial \bar{p}^n}{\partial x_i} \quad (9)$$

where $Res(\bar{u}^n)$, $Res(\bar{u}^{n-1})$ represent the convection and diffusion terms in (2) discretized on the time levels n and $n - 1$. The symbol u_{WALL} stands for the velocity at the wall which is a part of the computational domain as shown in Fig. 1 by black bold line. The velocity on that boundary is known and this allows to estimate the values of velocity in its closest vicinity, i.e. in the computational nodes shown in Fig. 1 by black squares. In the present approach the velocity in these nodes is obtained from a second-order linear interpolation based on the velocity values from the second node line from the boundary (shown by high arrow in Fig. 1) and the desired boundary values. Inside the immersed body, i.e. in the nodes with crosses, the velocity is set equal to zero.

3 Results

The accuracy of the SAILOR-IB code has been validated by computations of laminar flows in a lid-driven skewed cavity and over a backward facing step [13]. The obtained results were in very good agreement with the literature data obtained using the classical body fitted meshes. Most likely, in the present implementation the errors due to the approximate treatment of the walls are compensated by the high-order approximation far from the boundaries.

In this paper we deal with the turbulent flow in the converging–diverging channel in which the solution accuracy in near wall regions is of crucial importance. The computational domain for this test case is shown in Fig. 2. The dotted lines indicate the locations in which we will compare our results with DNS data obtained from Laboratoire de Mécanique de Lille (LML). The length of the domain (dimensionalised by a half domain height) is $L = 4\pi$, its height is equal to $H = 2$ and width is $W = 2\pi$. The computations are performed for $Re_\tau = u_\tau h/\nu = 395$ where u_τ is the friction velocity and $h = H/2$. At the inlet the fully developed turbulent flow is prescribed using the solution obtained from the simulations of periodic channel flow for the same Re_τ .

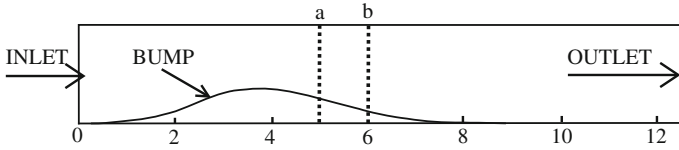


Fig. 2 Computational domain. The vertical dotted lines indicate the locations at which the solutions are compared with DNS data

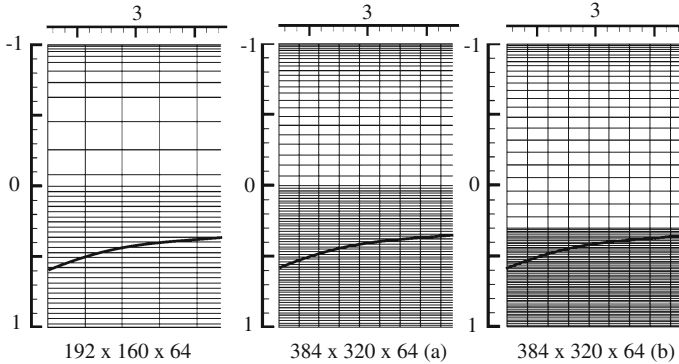


Fig. 3 Three types of the meshes used in the computations, every fourth grid lines are shown

The computational meshes used in the simulations consist of $192 \times 160 \times 64$ nodes and $384 \times 320 \times 64$ nodes. The denser mesh is additionally used with two different grid refinements. This is shown in Fig. 3 where additionally in a zoomed region of the bump the bold line shows location of the wall of the bump. The dense meshes will be denoted as (a) and (b). In all the cases, near the upper wall the grid nodes are distributed such that the first node is at $y^+ = 0.95$. On the bump side, the meshes are uniform and y^+ on the top of the bump is equal to 3.2 for the coarse mesh and 1.76 and 1.23 for the dense meshes (a) and (b), respectively.

3.1 Mesh Sensitivity Study

In this subsection, we analyse the influence of the mesh density based on the results obtained using the subgrid model proposed by Vreman. The reference DNS data were obtained on the mesh with $1536 \times 257 \times 384$ nodes which is approximately 77 and 20 times more nodes than in our coarse and dense meshes, respectively. Sample results obtained using the coarse mesh are presented in Fig. 4 showing an isosurface of the Q-parameter. It can be seen that the large turbulent scales vanish on the left-hand side of the bump and they reappear again on the falling side of the bump. This behaviour coincides with the regions where the flow accelerates and decelerates. These regions can be easily found in Fig. 5 showing instantaneous and time-averaged

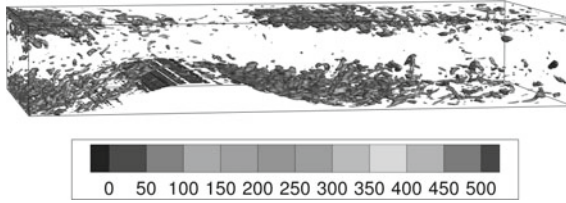


Fig. 4 Isosurface of Q-parameter ($Q = 2000(u_\tau/h)^2$) coloured by vorticity magnitude

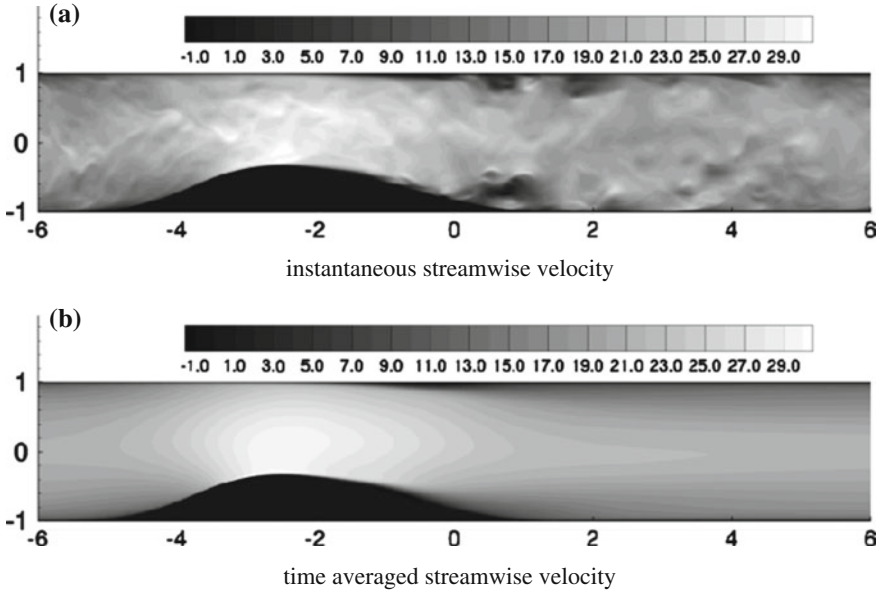


Fig. 5 Contours of the streamwise velocity normalised by u_τ : **a** mean values and **b** time-averaged values

contours of the streamwise velocity. We remind that in the IB method the velocity near the boundary of the bump is computed from the interpolation whereas in the nodes located inside the bump the velocity is explicitly set to zero every time step. Careful analysis of instantaneous velocity field near the wall of the bump shows small unphysical wrinkles. They are limited to the first two layers of the nodes, however they are not seen at all in the time-averaged solutions.

Detailed comparison and verification of the results are performed based on the velocity profiles at different locations in the channel. In all the cases the present solutions are very close to DNS data. In general, it cannot be said that the denser meshes provide significantly better results than using the coarse mesh. A sample comparison is presented in Fig. 6 showing the profiles of the mean and fluctuating components of the streamwise and the wall normal velocity along the line ‘a’ from Fig. 2. At this particular location it seems that the best solution is obtained using the dense mesh (a), though the results on the coarse mesh are also correct.

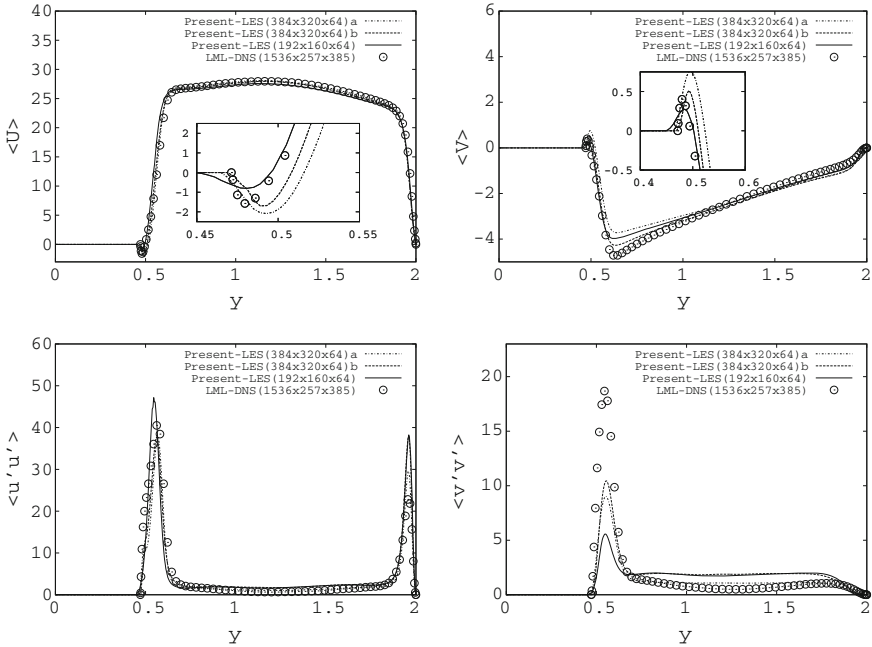


Fig. 6 Profiles of the streamwise and wall normal velocity components along line ‘a’

3.2 Comparison of the SGS Models

The comparison of the subgrid models is performed using the mesh $384 \times 320 \times 64$ (a). Figure 7 shows the contours of the total turbulent kinetic energy and the subgrid kinetic energy defined as $k_{sgs} = \frac{v_r^2}{(C_v \Delta)^2}$ with $C_v = 0.1$ [14]. These results were obtained using the σ -model but we note that the solution obtained using the Vreman model is very similar and practically indistinguishable by visual inspection. The maxima of kinetic energy are located in the regions of separation existing near the wall of the bump and close the upper wall. The ratio of k_{sgs} to the total kinetic energy is maximally 0.15. Hence, according to Pope’s criterion [15] the mesh used in these simulations ensure the proper resolution. Detailed comparison of the solutions is presented in Figs. 8 and 9. It can be seen that both subgrid models provide accurate and similar solutions and it cannot be said which one performs better. In the centre of the channel both the mean and fluctuating velocity profiles match the DNS results almost exactly. Only closer to the walls some discrepancies are observed. This can be caused by the IB method as well as by the errors due to the subgrid modelling. Nevertheless, it can be seen that the location of the velocity extrema in separation

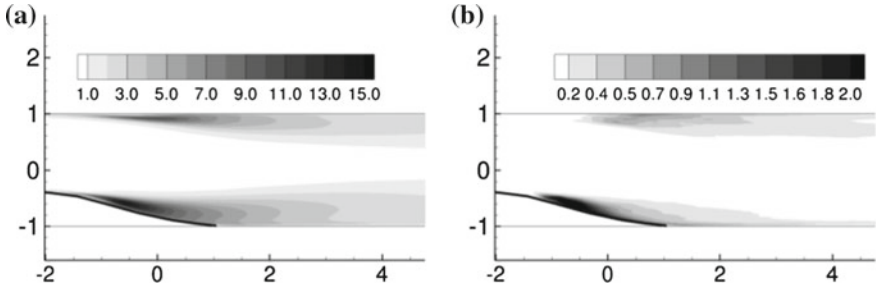


Fig. 7 Contours of the time-averaged subgrid and total kinetic energy. **a** Total turbulent kinetic energy. **b** Subgrid turbulent kinetic energy

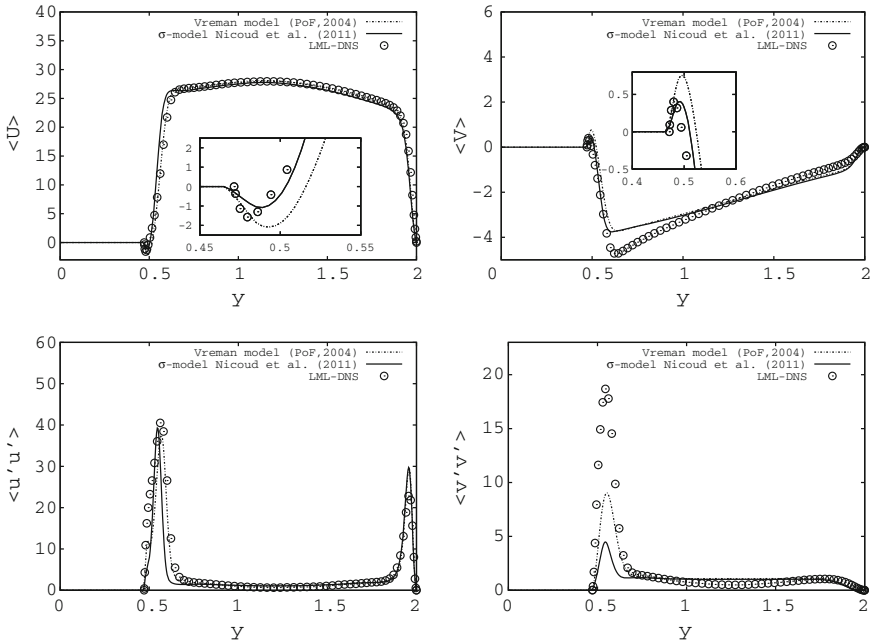


Fig. 8 Profiles of the streamwise and wall normal velocity components along the line 'a' obtained using two subgrid models

zones (the regions where the mean streamwise velocity near the walls is negative) is predicted relatively well by both models. The velocity fluctuations are also computed with good accuracy. Both the shapes of their profiles and their maximum values are close to DNS data.

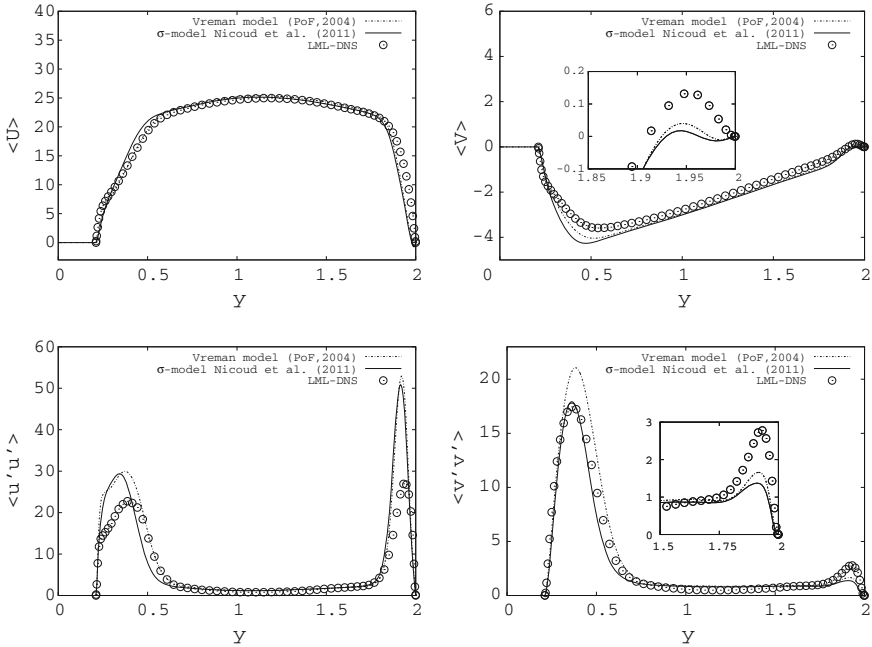


Fig. 9 Profiles of the streamwise and wall normal velocity components along the line ‘b’ obtained using two subgrid models

4 Conclusions

This paper shows results of flow modelling in a converging–diverging channel using LES combined with the Immersed Boundary (IB) method. With respect to exemplary literature DNS computations the application of LES allows significant reduction of the computational costs by using relatively coarse computational meshes. The use of the IB method allows to use the high-order code in the non-Cartesian computational domain without significant modifications of the solution algorithm. The LES computations were performed with the help of two subgrid models, proposed by Vreman [1] and Nicoud et al. [2] and in both the cases the obtained results were accurate. It could be seen that the better or worse agreement with DNS data was dependent on which quantity was compared and at which location in the channel. Hence, we conclude that both models are suitable for LES computations using IB method.

Acknowledgments Authors thank to Prof. W. Elsner for fruitful discussion. These research were supported by Polish National Science Centre under grant no. DEC-2012/07/B/ST8/03791. The computations were performed using PL-Grid Infrastructure (Poland).

References

1. A.W. Vreman, An eddy-viscosity subgrid-scale model for turbulent shear flow: algebraic theory and applications. *Phys. Fluids* **16**, 3670–3681 (2004)
2. F. Nicoud, H. Baya Toda, O. Cabrit, S. Bose, J. Lee, Using singular values to build a subgrid-scale model for large eddy simulations. *Phys. Fluids* **23**, 193–202 (2011)
3. C. Canuto, M.Y. Hussaini, A. Quarteroni, T.A. Zang, *Spectral Methods in Fluid Dynamics* (Springer, Berlin, 1988)
4. S.K. Lele, Compact finite schemes with Spektral-like resolution. *J. Comput. Phys.* **103**, 16–42 (1992)
5. T.K. Sengupta, A. Dipankar, A. Kameswara Rao, A new compact scheme for parallel computing using domain decomposition. *J. Comput. Phys.* **220**, 654–677 (2007)
6. S.K. Pandit, J.C. Kalita, D.C. Dalal, A transient higher order compact scheme for incompressible viscous flows on geometries beyond rectangular. *J. Comput. Phys.* **225**, 1100–1124 (2007)
7. L. Kuban, J.-P. Laval, W. Elsner, A. Tyliczszak, M. Marquillie, LES modelling of converging-diverging turbulent channel flow. *J. Turbul.* **13**, 1–19 (2012)
8. J. Mohd-Yosuf, Combined immersed-boundary/B-spline methods for simulations of flow in complex geometries. *Ann. Res. B. Cent. Turbul. Res.* (1997)
9. C.S. Peskin, Flow patterns around heart valves: a numerical method. *J. Comput. Phys.* **10**, 252–271 (1972)
10. B.J. Geurts, *Elements of Direct and Large-Eddy Simulation* (R.T. Edwards, Philadelphia, 2003)
11. R. Verzicco, G. Iaccarino, Immersed boundary technique for turbulent flow simulations. *Appl. Mech. Rev.* **56**, 331–347 (2003)
12. R. Mittal, G. Iaccarino, Immersed boundary methods. *Annu. Rev. Fluid Mech.* **37**, 239–261 (2005)
13. M. Ksiezzyk, A. Tyliczszak, Immersed boundary method combined with a high order compact scheme on half-staggered meshes. *J. Phys. Conf. Ser.* **530**, 012066 (2014)
14. S.B. Pope, *Turbulent Flows* (Cambridge University Press, Cambridge, 2000)
15. S.B. Pope, Ten questions concerning the large-eddy simulation of turbulent flows. *New J. Phys.* **6**, 35 (2004)